Materials Science & Engineering A xxx (xxxx) 141271

Contents lists available at ScienceDirect

Materials Science & Engineering A

journal homepage: www.elsevier.com/locate/msea

Microstructure and tensile properties of additive manufactured Ti-6Al-4V with refined prior-β grain structure obtained by rapid heat treatment

Zhiyi Zou [a], Marco Simonelli [a, *], Juliano Katrib [b], Georgios Dimitrakis [b], Richard Hague [a]

[a] Centre for Additive Manufacturing, University of Nottingham, Nottingham, NG8 1BB, UK
[b] George Green Institute for Electromagnetics Research Group, University of Nottingham, Nottingham, NG8 1BB, UK

ARTICLE INFO

Keywords:
Additive manufacturing
Titanium alloys
Rapid heat treatment
Tensile properties

ABSTRACT

Heat treatments tailored for additive manufactured Ti-6Al-4V can be used to attain desirable microstructures associated with superior mechanical properties. Rapid heat treatments, for example, can be used to recrystallise the microstructure of laser powder bed fusion (L-PBF) Ti-6Al-4V to obtain refined and quasi-equiaxed prior-β grains. In this study, we discuss the interplay between refined microstructures and the tensile properties of Ti-6Al-4V specimens. The influence of individual microstructural constituents on the tensile properties are examined in detail and directly compared to those found in specimens subject to conventional annealing treatments. It was found that rapid heat treatments into the β phase field can significantly refine the size of the prior-β grains found in as-built L-PBF Ti-6Al-4V, as well as alter the size and morphological arrangement of the resulting α laths. The proposed new heat treatments are clearly shown to have strengthened the alloy with no apparent detriment to the ductility of the material.

1. Introduction

As one of the most popular titanium alloys, Ti-6Al-4V presents as a material with high specific strength alongside excellent corrosion resistance and biocompatibility; this therefore leads to a wide range of applications in the aerospace, medical, automotive and chemical industries [1–3]. Over the past decade, laser powder bed fusion (L-PBF) of Ti-6Al-4V has attracted significant attention as a promising manufacturing approach, due to its ability to produce net-shape components of complex geometry with minimal material waste [4,5].

Substantial insights into this manufacturing approach have been provided thanks to a significant body of related research. It has previously been extensively demonstrated that by carefully optimising the process parameters and minimising the use of recycled powders, Ti-6Al-4V can be printed to form high quality parts with minimal microstructural defects, such that it is possible to reach near full density components [6–8]. However, even using optimised processing parameters, large variability is observed in the mechanical properties of as-built parts [7,9–11]. This is because these properties are simultaneously affected by various microstructural features, such as the dimension of the prior-β grains and the morphology and size of the α/α' phase, each of them being laser-parameter dependant [12,13].

Therefore, post-process heat treatments are routinely performed to create a uniform microstructure of L-PBF Ti-6Al-4V, reduce property variation and inform robust material models [14–17].

Typically, heat treatments utilised on L-PBF Ti-6Al-4V components follow from the body of knowledge developed for thermo-mechanical processing. However, this does not take into consideration the specific microstructural attributes imparted by additive manufacturing, which might include grain size inhomogeneities, location-specific residual stresses and microstructural anisotropy [14]. As an example, the ASTM F2924-14 and F3001-14 standards suggest heat treatments to be conducted within the high portion of the α + β phase field below the β-transus temperatures [18,19]. While these high-temperature heat treatments are effective to eliminate residual stress and recover the microstructure of Ti-6Al-4V, they are ineffective in refining the microstructure of the printed materials [15,16,20]. As a result, microstructural anisotropy persists, affecting mechanical properties such as ductility, fracture toughness and fatigue [21,22]. Alternative heat treatments tailored to L-PBF Ti-6Al-4V could enable the attainment of superior properties owing to the unusual starting microstructure found in the as-printed components. Zhao, Chen, Tan, Zhang, Lin and Huang [23], for example, annealed L-PBF Ti-6Al-4V at a temperature (980 °C) extremely close to the β transus temperature prior to the traditional heat treatment routine, to trigger globurisation of the α phase

* Corresponding author.
E-mail address: Marco.Simonelli@nottingham.ac.uk (M. Simonelli).

https://doi.org/10.1016/j.msea.2021.141271
Received 17 November 2020; Received in revised form 8 April 2021; Accepted 10 April 2021
0921-5093/

which directly contributed to ductility enhancement. Another specially-designed heat treatment for L-PBF Ti-6Al-4V was proposed by Sabban, Bahl, Chatterjee and Suwas [24], where the authors thermally cycled L-PBF Ti-6Al-4V in a temperature range close to the β transus temperature (between 975 °C and 875 °C) for 24h, to attain globurisation of the α phase and ductility improvements. In these two studies, globurisation is explained as a response of the inherent dislocation sub-structure naturally present in the martensitic phase of the printed material from the thermal treatment [23,24]. In an effort to reduce microstructural anisotropy, other work has demonstrated that it is possible to obtain equiaxed β grains by conducting heat treatments above the solid phase transformation temperature in Ti-6Al-4V, also known as the β-transus temperature [16,20,25]. However, an unacceptable loss in strength and ductility was observed, owing to the extensive β grain growth during such heat treatment [16,20]. In a recent investigation, the authors demonstrated the benefits of using rapid heat treatments (RHT) to refine the prior-β grain structure via epitaxial recrystallisation, and it was suggested that RHTs could improve the mechanical properties of the L-PBF Ti-6Al-4V [5].

Although recently published work has demonstrated the specific advantages of tailored heat treatments for L-PBF Ti-6Al-4V, it is still unclear what is the most favourable microstructural arrangement for enhancing specific mechanical properties and which heat treatment can deliver such microstructure. This study aims at elucidating the role of individual microstructural constituents, and in particular the size of the prior-β grains, on the tensile properties of L-PBF Ti-6Al-4V to define a heat treatment protocol capable of providing a superior combination of strength and ductility.

2. Material and methods

2.1. Materials used in this study

The materials used in this study were Ti–6Al–4V (grade 23) cylinders of 9 mm diameter and 60 mm length produced by L-PBF at 90° build angle to the build platform. The produced cylinders were supplied by 3T Additive Manufacturing Ltd, manufactured on an EOSINT M290 using proprietary optimised process parameters.

The chemical compositions of the as-built material were examined at various locations by Energy-Dispersive Spectroscopy (EDS) in a Hitachi TM 3030 Scanning Electron Microscope (SEM). Results suggest that the material consists of an average of 90.9% Ti, 5.7% Al and 3.3% V (wt.%) well within the nominal composition range of typical Ti-6Al-4V. The β transus temperature of the as-built material, i.e. the lowest equilibrium temperature which maintains the entire material in the β phase, was ascertained by Simultaneous Thermal Analysis (STA) using a TA Instruments TGA-SDTQ600 analyser. Results suggest an average measured β-transus temperature of 1013 ± 5 °C.

2.2. Heat treatments of the as-built materials

In order to examine the impact of the various microstructural constituents, and in particular the size of the prior-β grains on the tensile properties of Ti-6Al-4V, specimens were subject to specific heat treatments as summarised in Table 1. The first heat treatment – hereafter name as "CHT" (conventional heat treatment) – was carried out to establish the benchmark tensile properties of the materials used in this study. For the CHT, samples were vacuum-sealed (O_2 level < 10 ppm) in silica ampoules and then treated in a commercial muffle furnace. Samples were heated at 10 °C/min and annealed at 925 °C for 2 h then subsequently aged at 700 °C for 4 h. CHT was then followed by air cooling (average cooling rate of about 7 °C/min). For the rapid heat treatments, a bespoke induction heating setup operating within an Argon atmosphere was used [5]. This experimental set up allowed a constant heating rate of 10 °C/s to a target temperature around 1000 °C and a short dwell time in the range of seconds before cooling the samples at room temperature by Argon convection. Four distinct rapid heat treatment were investigated (hereafter RHT1 to RHT4) with a total of 5 samples per heat treatment type. Where ageing was conducted, samples following RHT were encapsulated in silica ampoules and then aged in a furnace. For all the heat treatments, the cooling rates reported are the average cooling rates from the soaking temperature to 400 °C prior to any ageing.

Table 1
Summary of the five different heat treatments applied in this study.

Assigned name	Heating rate	Soaking temperature and time	Cooling rate	Ageing
CHT	• 10 °C/min	• 925 °C • 2h	• 7 °C/min	Yes
RHT1	• 10 °C/s	• 980 °C • 1s	• 4 °C/s	Yes
RHT2		• 1005 °C • 1s		Yes
RHT3		• 1030 °C • 1s		Yes
RHT4		• 1030 °C • 1s		No

2.3. Microstructural characterisation

The microstructural constituents of the material under different conditions were examined using X-ray Diffraction (XRD) via a Bruker D8 ADVANCE device with the DAVINCI XRD system. The observation of the typical microstructural features was carried out on the frontal plane (XZ surface) of the specimens using a Nikon Optiphot 100 optical microscope and a JEOL 6060LV SEM. Where needed, the average width of the prior-β grains was measured using standard mean linear intercept methods [26,27] on optical microscopy images, while the average thickness of the α lath was measured using the modified mean linear intercept methods, recommended by Vander Voort and Roósz [26], directly on backscattered electron microscopy images.

The crystallographic texture of the specimens was investigated via Electron Back-Scattered Diffraction (EBSD) through a JEOL 7100F FEG-SEM with a step size of 0.5 μm, also on the frontal plane (XZ surface) of the specimens for consistency. The collected data was analysed using OIM^R and the MATLAB toolbox Mtex-5.1.1. All inverse pole figures are colour coded with RD parallel to build-direction (z-axis). Where needed, the β-phase at the high temperature was reconstructed by back-calculation from the room temperature α/α′ phase via the Burger Orientation Relationship (BOR) as described in Ref. [28]. During the reconstruction, each reconstructed β grain derived from a minimum of four distinct, but contiguous, α/α' variants, with a further constraint on the maximum misorientation angle permitted across one reconstructed β grain of 10°.

2.4. Tensile testing

Tensile specimens with a diameter of 4 mm and a gauge length of 20.4 mm were machined from the centre of the printed cylinders, according to standard ASTM E8/E8M – 16a [29]. Tensile tests were then conducted at room temperature on an Instron 5969 at a displacement rate of 0.14 mm/min. The test direction was parallel to the build-direction (z-axis) of the Ti-6Al-4V cylinders.

3. Results

The microstructure of L-PBF Ti-6Al-4V under different conditions (as-built and after various heat treatments) are described in section 3.1, including the phase constituents, morphological characteristics and

crystallographic texture. The corresponding tensile properties in each condition are reported in section 3.2. The influence of individual microstructural constituents on the tensile properties of L-PBF Ti-6Al-4V are discussed in section 4.

3.1. Microstructure of L-PBF Ti-6Al-4V subject to different heat treatments

3.1.1. Phase constituents in as-built and heat-treated L-PBF Ti-6Al-4V

Fig. 1 demonstrates the microstructural constituents under different conditions measured via XRD analysis. The XRD spectrum suggests the presence of only the hexagonal close-packed (hcp) phase in the as-built specimen. For Ti-6Al-4V, the hcp pattern can be a result of either α-phase or martensitic α′, as they all share the same crystalline structure and have similar lattice parameters [30,31]. Considering the fast cooling (in excess of 10^4 °C/s) of the melt pool during L-PBF processing, the hcp microstructure in Fig. 1 is interpreted as α'. Therefore, the martensitic α' is the only detectable phase present at room temperature for as-built L-PBF Ti-6Al-4V, i.e. the starting microstructure of the samples prior to the heat treatments. No β-bcc phase was detected by XRD, however, due to the low resolution of XRD, this does not rule out the existence of undetected nanoscale β phase in the as-built microstructure.

After different heat treatments, a resemblance in the XRD patterns of the samples is recognised, as signal peaks are detected at identical 2θ angles (2Theta) in each condition. All XRD patterns reveal a combination of hcp phase and bcc phase. The bcc pattern represents the β phase,

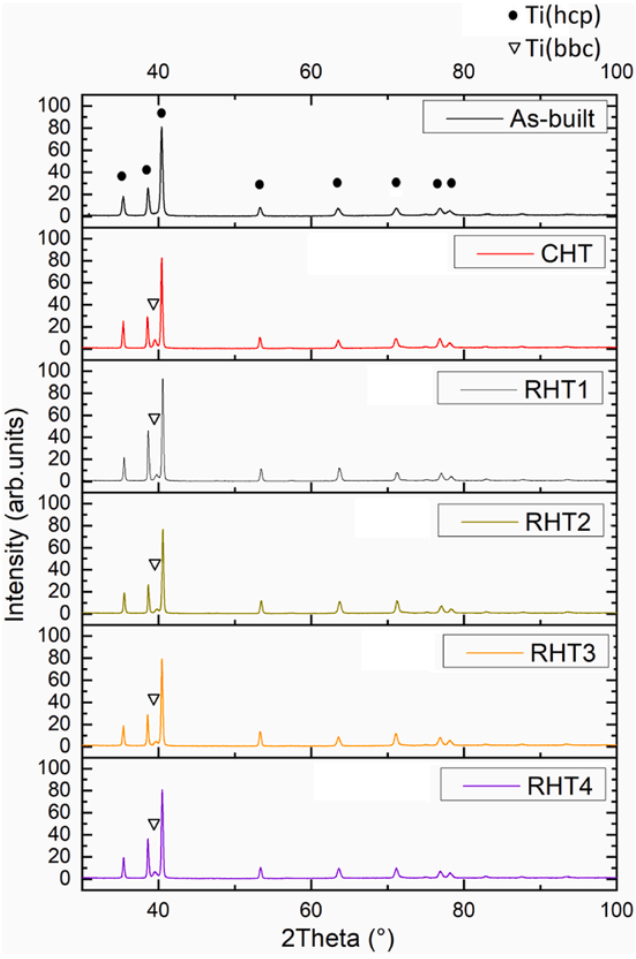

Fig. 1. XRD spectra obtained from L-PBF Ti-6Al-4V subject to different heat treatments. Marked by an inverted triangle is the distinctive (110) reflection of the β phase of Ti-6Al-4V.

which is clearly characterised by the (110) reflection as marked in Fig. 1. The hcp pattern is interpreted as α phase, considering the fact that the cooling rate experienced in all conditions, (7 °C/min for conventional HT and 4 °C/s for RHTs) is well below the critical cooling rate (20 °C/s) to trigger any either martensitic or massive α phase transformations.

3.1.2. Morphological changes of the prior-β grains as a function of heat treatment

Optical microscopy images that demonstrate the typical morphology of the prior-β grains in the samples prior to and after different heat treatment are presented in Fig. 2. The measured average widths of the prior-β grain in each condition are reported in Table 2. Columnar prior-β grains extending along the build direction can be observed in as-built L-PBF Ti-6Al-4V, as shown in Fig. 2 (a). The average measured width is 83.8 ± 8.3 μm. It is well understood that the columnar morphology is a result of the directional heat loss and the successive layer deposition during the printing process [32]. After CHT, the columnar morphology of the prior-β grain persists (Fig. 2b), and the measured average width is 87.1 ± 10.9 μm, similar to that observed in the as-built condition.

After each of the RHTs, the columnar morphology of the prior-β grains develops into a refined quasi-equiaxed morphology. Such development can be observed qualitatively in the optical microscope images (Fig. 2 (c)–(f)), and is quantified in terms of reduction in the measured average grain width in Table 2. A suggested mechanism that can lead to the observed refinement is discussed in our previous work, where it is proposed that epitaxial recrystallisation could take place during RHT [5]. In particular, it is thought that the high density of dislocation in the as-built microstructure would initiate epitaxial recrystallisation of α sub-grain inside the original prior-β grain. The newly formed recrystallised β are highly misoriented with respect to the surrounding recovered β and therefore their growth during RHT reduces the overall texture and columnar morphology observed in the micrographs [5]. Additionally, RHTs expose the specimens to high temperatures (near or above the β transus temperature) for a short duration, greatly limiting the growth of the β phase and therefore allowing the preservation of a refined recrystallised structure upon cooling [5].

The transition of columnar to quasi-equiaxed prior-β grains is maximum when the peak temperature of the RHT exceeds the β transus temperature, with RHT2 to RHT4 all showing comparable prior-β grain widths. When the peak temperature is close, but lower, than the β transus temperature (RHT1), columnar grains are observed to persist, suggesting that the remnants of the α phase may pin, at least partially, the original prior-β grain boundaries, thus resulting in a limited morphological change of the β during the heat treatment.

The average prior-β grain size achieved after RHT is not only significantly smaller than the original as-built status but also considerably smaller than that reported in a number of studies where the microstructure of L-PBF Ti-6Al-4V (printed on similar EOS platforms) was investigated (Table 3) [33–37].

3.1.3. Morphological changes of the α and β phases as a function of heat treatment

The morphology of the α and β phases in L-PBF Ti-6Al-4V is also significantly influenced by the different heat treatments. The starting microstructure within the prior-β grain in the as-built condition, as revealed in Fig. 2 (a) and (b), is fine, acicular α′ needles with an average thickness close to 1 μm. The interweaved pattern of α′ martensite suggests a concurrent growth of different variants during cooling [32]. After CHT, the microstructure within the prior-β grain develops to multi-crossover α and β lamellae, as characterised in Fig. 3 (c) and (d), forming a typical basketweave arrangement. The literature suggests that when α′ martensite decomposes during the heat treatment, the α phase will be first nucleated within the acicular α′

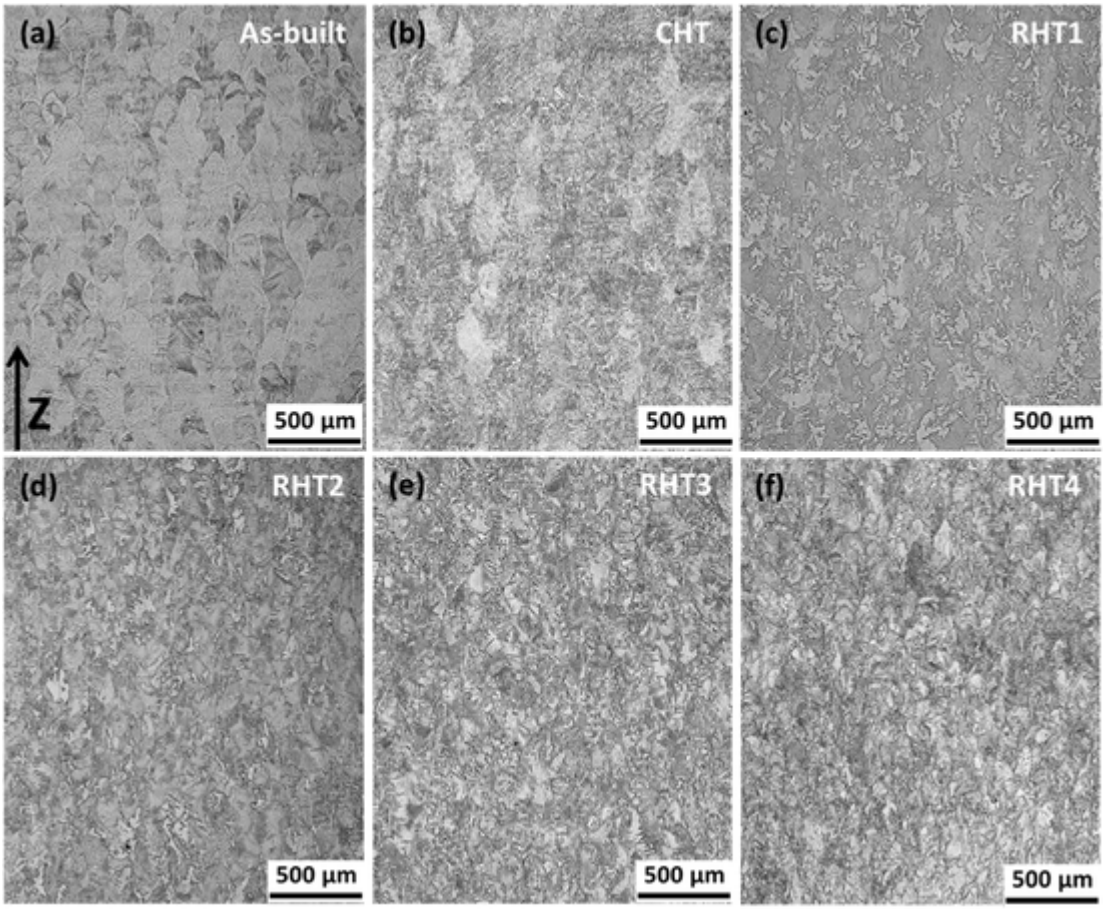

Fig. 2. Optical microscope images that show the typical morphology of the prior-β grains after different heat treatments: (a) as-built and following, (b) CHT, (c) RHT1, (d) RHT2, (e) RHT3 and (f) after RHT4. Both specimens in as-built condition and after conventional HT present columnar prior-β grains parallel to the build direction, while all specimens after RHTs display a refined quasi-equiaxed morphology.

Table 2
The measured average width of the prior-β grains after different heat treatments.

	As-built	CHT	RHT1	RHT2	RHT3	RHT4
Results (μm)	83.8 ± 8.3	87.1 ± 10.9	40.6 ± 9.5	34.3 ± 5.1	36.1 ± 8.0	31.9 ± 3.9

Table 3
Average prior-β grain size reported in related studies of L-PBF Ti-6Al-4V printed on EOS platforms.

Source	The average width of the prior-β grain (μm)
Wilson-Heid, Wang, McCornac and Beese [37]	96.3 ± 18.0
Neikter, Åkerfeldt, Pederson, Antti and Sandell [35]	87 ± 10
Tao, Zhong, Li, Hu, Gong and Xu [33]	139.7 ± 11.2
Dilip, Zhang, Teng, Zeng, Robinson, Pal and Stucker [36]	80 – 200

phase following an expected recovery mechanism [15]. During this process, vanadium would diffuse from the newly formed α phase and be concentrated at the α phase boundary [15]. Such element partitioning then leads to the formation of β phase in the vanadium-rich area between α lamellae [15]. The elements partitioning can be evidenced by the different contrast showing in the SEM images (Fig. 3 (c) and (d)), where the vanadium enriched area has a lighter appearance. Consequently, the interweaved pattern of the as-built α' martensite is expected to be eventually replaced by the observed interlaced arrangement of α and β lamellae.

Lamellae of the α phase with an average thickness of 1.4 ± 0.1 μm can be clearly characterised in Fig. 3 (c) and (d), which presents a significant coarsening when compared with the thickness of the initial α' martensite (smaller than 1 μm). The observed coarsening is believed to be driven by the reduction of interfacial energy and the competitive growth between α and β phases at high temperature [15]. This mechanism can also be evidenced by the presence of apparent equiaxed α grains, indicated by white arrows in Fig. 3 (d). The change in morphology of the α phase during heat treatment has been the subject of ongoing investigations and might be related to the globularising phenomena described in related literature [23,24], or associated with the growth of the α that is perpendicular to the observed surface.

After each of the applied RHT, parallel lamellar α + β is identified to be the predominant structure within prior-β grains in all specimens, as presented in Fig. 4. The average thickness of the α lath measured in each condition is summarised in Table 4. The average thickness of the α lath after RHTs is clearly smaller than that after conventional HT (0.6 μm vs 1.4 μm). Continuous grain boundary α with an average thickness of about 2–3 μm can also be observed at each specimen, as indicated by the white arrows in Fig. 4. These features, not present either

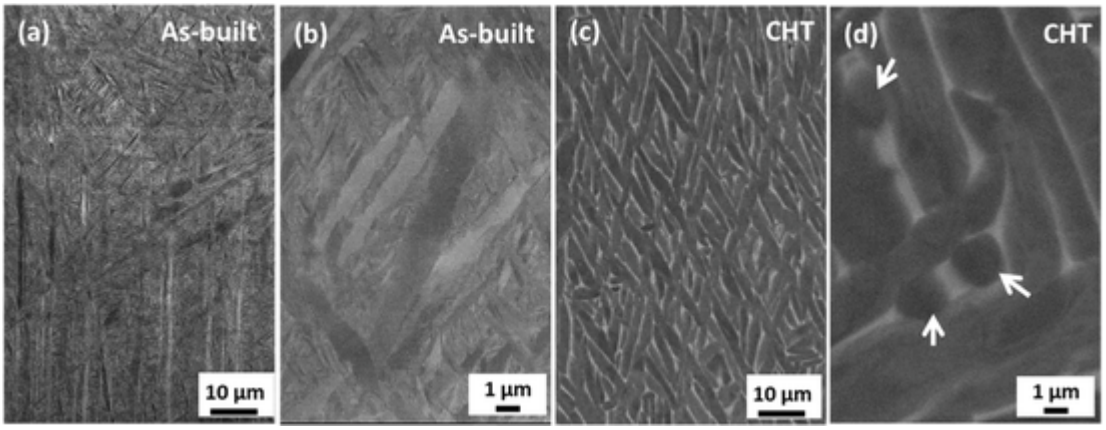

Fig. 3. Backscatter electron images that demonstrate the typical morphology of the α and β phases before and after CHT: (a) (b) Details of the fine acicular α′ martensite in the as-built condition, (c) Interweaved lamellar α + β after conventional HT, (d) After conventional HT, coarsening of α lamellae can be observed, as well as the appearance of apparent-equiaxed α phase, indicated by white arrows.

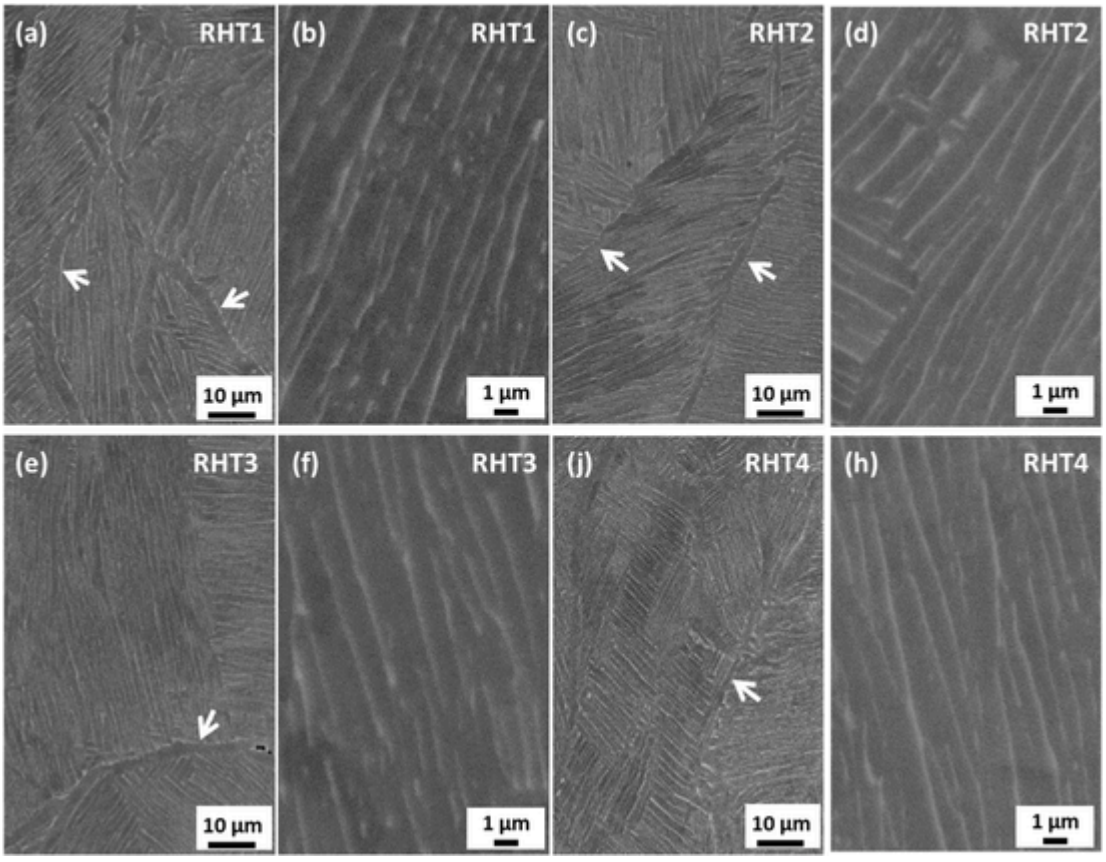

Fig. 4. Typical arrangement of the α and β phases in (a) (b) RHT1, (c) (d) RHT2, (e) (f) RHT 3, (j) (h) RHT4. The α and β phases display a predominant parallel morphological arrangement. Continuous grain boundary α also appears at the prior-β grain boundaries, as indicated by white arrows.

Table 4
The measured average thickness of the α laths after different heat treatments.

	CHT	RHT1	RHT2	RHT3	RHT4
Results (μm)	1.4 ± 0.1	0.7 ± 0.1	0.6 ± 0.1	0.6 ± 0.1	0.6 ± 0.1

in the as-built or after CHT, presumably originate because of the relatively slow cooling rate from the β phase (approximately 4 °C/s) associated with the proposed RHTs.

3.1.4. *Crystallographic texture evolution after heat treatment*

The crystallographic texture of the as-built specimen is presented via phase orientation maps in Fig. 5. It can be observed from the α-orientation map in Fig. 5 (a) that 5 to 7 α′ variants are present within each prior-β grain. This might suggest that α' variant selection might take place during the solidification of L-PBF process. Such a selection process might be influenced by multiple factors such as high cooling rates and localised strain accommodation principles, as described in

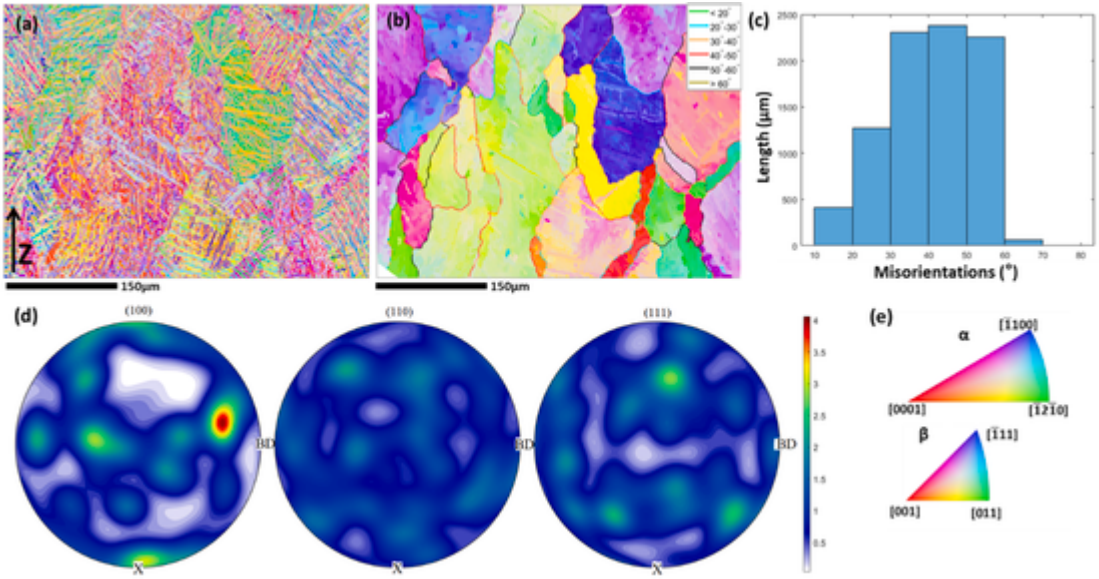

Fig. 5. Typical crystallographic texture of the as-built specimen: (a) Z-IPF α-orientation map and (b) reconstructed β-orientation map using the same colour-code; (c) misorientation distribution across reconstructed β grains; (d) contour pole figures showing the β texture, where BD stands for building direction; (e) colour scheme used in the maps. (For interpretation of the references to colour in this figure legend, the reader is referred to the Web version of this article.)

Refs. [38,39]. The texture of the elongated prior-β grains in the reconstructed β-orientation map, as shown in Fig. 5 (b), supports the observations conducted from optical microscopy in section 3.1.2. The distribution of the calculated β grain boundary angles is presented via the histogram shown in Fig. 5 (c) as well as the colour-coded boundaries in the orientation map of Fig. 5 (b). The β grain boundary angles spread between 10° and 70°, with moderate occurrence in a wide range between 30° and 60°.

After CHT, the coarsened α lamellae can be clearly characterised from the α-orientation map in Fig. 6 (a), while the reconstructed β-orientation map reported in Fig. 6 (b) shows a typical elongated columnar morphology of the prior-β grains. The distribution of β grain boundary angles shown in Fig. 6 (c) is similar to that measured in the as-built condition. It is also noted that during this heat treatment, no recrystallisation takes place, as demonstrated by the fact that no change in the distribution of the β grain boundary angles is noted between as-built and conventional HT samples.

Specimens after RHT1 presents a crystallographic texture significantly different from the samples subject to CHT, as shown in Fig. 7. Instead of the individual α/α' laths observed in α-orientation map from as-built and conventional HT conditions, α colonies are clearly apparent in Fig. 7 (a). This suggests that the parallel α lamellae observed within each of the prior- β in Fig. 4 (a) and (b) possess most likely similar crystallographic orientation. The refinement and the morphology of the prior-β grains can be further evidenced by the reconstructed β-orientation map in Fig. 7 (b). The distribution of β grain boundary angles is shifted towards higher angles, as shown in Fig. 7 (c), as most of the β grain boundary angles (57.5% in total length) are spread in a limited range from 50° to 60°. Such development in the boundary angle

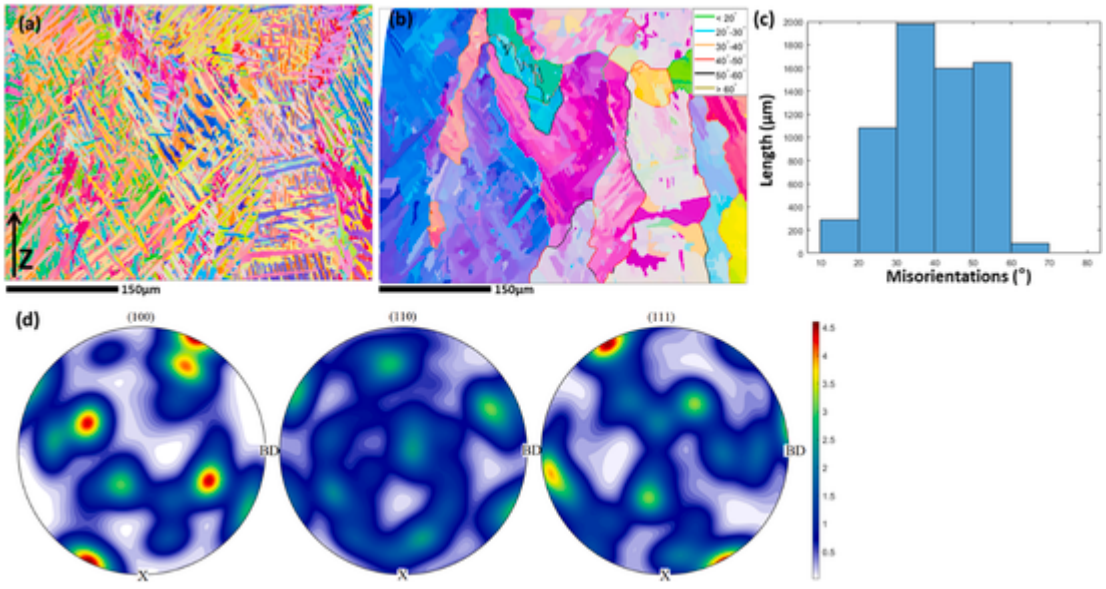

Fig. 6. Typical crystallographic texture of the specimen after CHT: (a) Z-IPF α-orientation map of L-PBF Ti-6Al-4V after furnace treated at 925 °C for 2 h then ageing treated at 700 °C for 4 h; (b) Corresponding reconstructed β-orientation map; (c) The misorientation distribution across reconstructed β grains; (d) contour pole figure of the β texture.

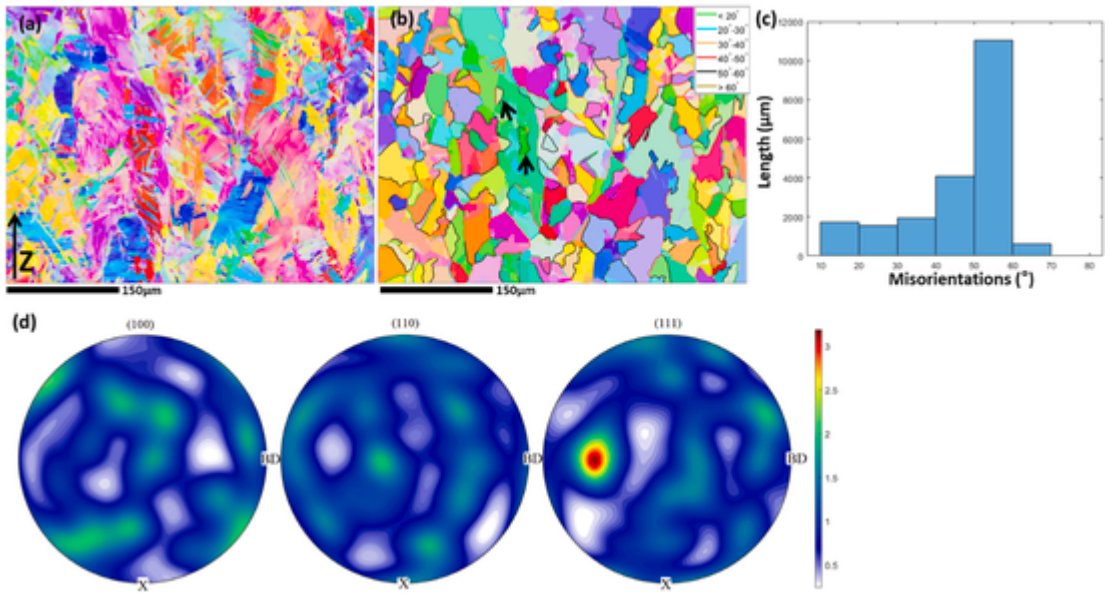

Fig. 7. Typical crystallographic texture of specimens subject to RHT 1: (a) Z-IPF α-orientation map; (b) Corresponding reconstructed β-orientation map. Black arrows indicate small HAB grain boundaries located in the centre of the columnar grain; (c) The misorientation distribution across reconstructed β grains; (d) contour pole figure of the β texture.

distribution suggests that recrystallisation took place at a significant scale during the adopted RHTs.

As reported in Section 3.1.2, a mixture of quasi-equiaxed and columnar prior-β grains is evinced from Fig. 7b. Interestingly, distinct small grains can be observed within columnar grains, as indicated by the black arrows in Fig. 7b. The high angle boundary (HAB) characteristic of such small grains corroborates the hypothesis that the observed grain refinement is associated with the recrystallisation phenomena. Considering the complexity of microstructure's component produced in additive manufacturing, there is the possibility that, in 2D sectional EBSD mapping, prior-β grains could appear inside another prior-β grain. Such a phenomenon can be observed in Figs. 5b and 6b. It can be noted that those prior-β grains, although appearing inside another grain, still present a coarse morphology, the size of which are significantly larger than the specific β grains (highligted by black arrows in Fig. 7b). Considering the coarse nature of prior-β grain acquired during AM process, the much smaller β grains in Fig. 7b are interpreted as the result of recrystallisation during heat treatment.

The crystallographic texture of the samples following the remaining RHTs is presented in Fig. 8 and Fig. 9. Similar to that observed in Fig. 7, α colonies dominate all of the α-orientation maps, while refined quasi-equiaxed prior-β grains with HAB are present in the reconstructed β-orientation maps. In all three conditions, it is observed a predominance of high angle β grain boundary. Additionally, the images confirm that the prevalent morphology of the prior-β grains is quasi-equiaxed, marking a significant difference to that observed in the samples following conventional heat treatment .

3.2. Tensile properties of L-PBF of Ti-6Al-4V after conventional and rapid heat treatment

Significant differences between the microstructure of L-PBF Ti-6Al-4V after CHT and RHTs suggest the specimens may present a different behaviour during the tensile test. The tensile test results after different treatments are reported in Table 5, while the stress-strain curves of all the conducted tensile tests are displayed in Fig. 10.

Although no specific trend is observed in the elastic modulus of the materials, suggesting that these are essentially independent of microstructure when a weak texture of the α phase is present, several differences can be observed in the yield onset and the following plastic deformation of the materials. As-built specimens present a typically high strength (both yield stress and UTS) and low ductility. CHT, enhance the ductility of the samples significantly, and elongations exceeding 15.9% can be obtained. A typical debit in strength is however observed. The specimens subject to RHT2 and RHT3 possess similar values of elongation but with higher yield stress and ultimate tensile strength. Finally, samples after RHT1 and RHT4 possess similar tensile properties to that observed in the specimens following CHT with no significant differences in neither strength or ductility. However, the duration required to conduct the CHT treatment is 12 h, while RHT4 can be completed in 20 min, thereby offerring clear processing cost reductions.

In addition to the significant reduction of the process duration, the columnar morphology of the prior-β grains after CHT treatment suggests the presence of anisotropy behaviours, while equiaxed grains induced by RHT suggest the potential to generate specimens with isotropic characteristics.

4. Discussion

The tensile properties of Ti-6Al-4V result from of a complex response of how several microstructural features interplay during deformation. The mechanical behaviour of as-built samples has been previously studied [15,40,41] and is largely characterised by the limited deformation that the martensitic α′ phase can sustain. Authors have demonstrated that the exceptional high strength/low ductility of the as-built material derives from the large concentration of vanadium (which provides substantial solute strength [42]) and the high dislocation density typically found in the α′ phase [41]. Additionally, it has been suggested that thin nano-stripes of β phase (not usually detected by XRD and only revealed by detailed TEM investigations) might be retained between α' martensitic laths [43] and further limit the plasticity of the martensitic phase by acting as stress concentration spots at the boundary between the two phases [43].

After CHT and RHT, the α' martensite decomposes into α + β, as discussed in section 3.1.3 [44]. The deformation of these microstructures is more complex and influenced by a number of factors, including how strain partitions across the two phases, the thickness of individual α laths, the lath arrangement (either as basketweave or as colonies), differences prior- β grain sizes and the presence of grain boundary α

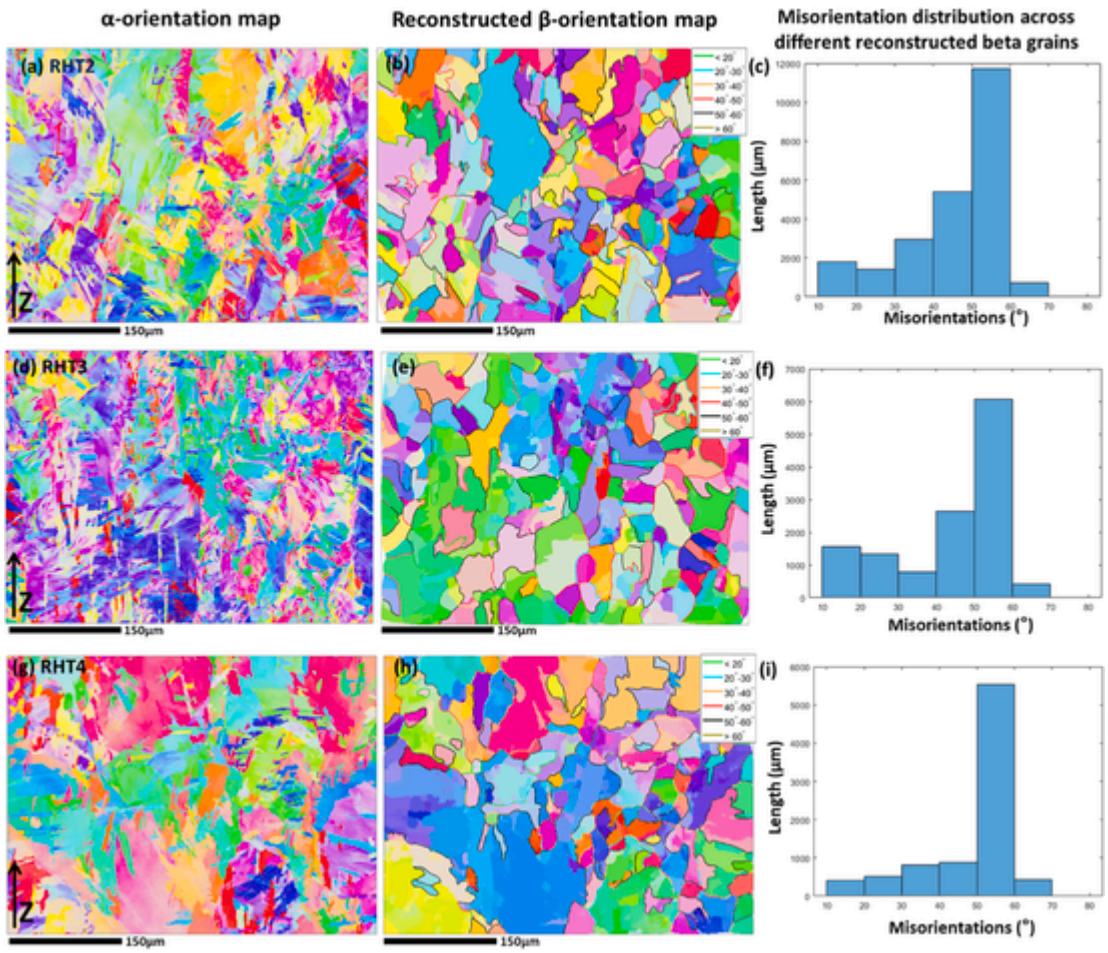

Fig. 8. Typical crystallographic texture of specimens subject to different RHT. For each condition, a Z-IPF α-orientation map, a corresponding reconstructed β-orientation map and the misorientation distribution across reconstructed β grains are displayed. (a) (b) (c), RHT2; (d) (e) (f), RHT3; (g) (h) (i), RHT4.

[45–47]. Microstructural features found in these two conditions are summarised in Table 6.

EBSD and XRD measurements indicate a similar volume fraction of the α and β phase in the samples treated by CHT and RTH. Any phase fraction variation, if present, is therefore expected to lead to a negligible impact on the measured tensile properties. After heat treatment however, specimens exhibit different size and morphological arrangement of the α and β phases.

Specimens after CHT maintain a favourable basketweave α lath arrangement, which is strictly inherited from the as-built microstructure. In the basketweave α arrangement, slip transmission is greatly reduced between adjacent α laths of different orientations, contributing directly to the overall strength of the alloy. The basketweave strengthening factor is well described by the Taylor hardening model and has been shown to be an important strengthening contributor in the as-printed and stress-relieved AM Ti-6Al-4V [4]. This is in stark contrast to the α arrangement found in the RHT'd samples – which were cooled directly from the β phase with moderate cooling rates and for which α colony arrangements predominate. In these samples, strength derives mostly from the interfacial strengthening effect that derives from the interface between the α and β phases which effectively acts as a microstructural barrier to slip transmission [45,48]. This microstructural arrangement is well modelled by Hall-Petch type equations where a decrease in the equivalent α lath thickness (often assumed as the size of the α-colony) can result in an increase of the alloy strength [49].

It is generally accepted that the properties of Ti alloys depend on the grain size of the high temperature β phase, with smaller grain size - such as those achieved after the investigated RHT - leading to better tensile properties [50]. For example, Both Lee [47] and Chong, Bhattacharjee, Yi, Shibata and Tsuji [51] observed an increase in both of the strength and ductility of Ti-6Al-4V as the prior-β grain size was decreased. Such improvements - loosely explained by the Hall-Petch relationship - are rationalised considering the role of the cumulative grain boundary length, which is maximised in refined microstructures. Recent research suggests that early stage strain localisation in high aspect ratio alpha grains could extend throughout prior beta grain boundaries [52]. Such grain boundary strengthening mechanisms could also be exploited by our proposed refined microstructures.

Additionally, refined microstructures such as those obtained after RHT decrease the overall softening effect caused by otherwise strong β textures that form during L-PBF Ti-6Al-4V, which in conjunction with the Burger's orientation relationship, are known to cause the softest slip systems to be placed at locations where resolved shear stress is highest [4]. The refined β grains observed in the RHT'd samples are however decorated by continuous grain boundary α, which is a distinctive microstructural feature associated with β to α phase transformations taking place at relatively low cooling rates. Grain boundary α are generally considered deleterious to the tensile properties of titanium alloys as they are softer than the surrounding α + β matrix [53] and therefore are thought to have impacted negatively on the observed strength of the RHT'd specimens. It is therefore highly relevant to observe that the RHT'd samples, although lacking a favourable basketweave α arrangement, can still display increased strength.

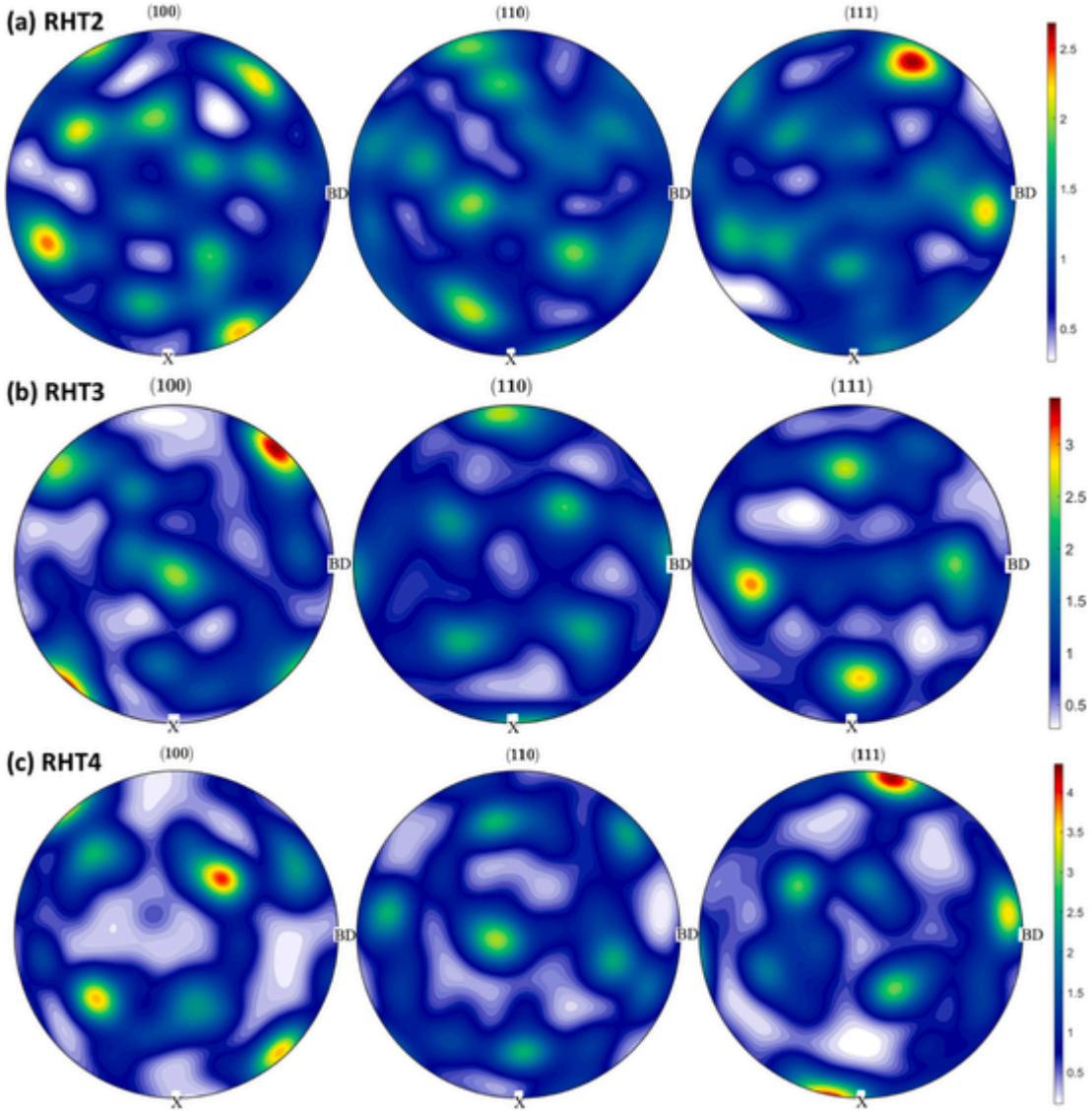

Fig. 9. Typical textures of specimens subject to different RHT. Contour pole figures representing the β texture display the (a) RHT2; (b) RHT3; (c) RHT4 conditions respectively.

Table 5
Tensile properties for each of the tested conditions, reported in the form of mean value +/-standard deviation.

	Young's modulus E (GPa)	Yield stress σy (MPa)	UTS (MPa)	Elongation ε (%)
As-built	124 ± 1	1123 ± 6	1242 ± 5	5.2 ± 0.2
CHT	121 ± 2	833 ± 13	913 ± 13	15.9 ± 0.8
RHT1	117 ± 2	831 ± 10	914 ± 10	15.9 ± 1.0
RHT2	118 ± 2	858 ± 14	937 ± 12	16.0 ± 1.1
RHT3	121 ± 1	854 ± 11	934 ± 11	16.6 ± 0.7
RHT4	118 ± 1	832 ± 9	940 ± 10	15.4 ± 0.8

Lastly, it is noteworthy that the specimens which experienced ageing show higher strength regardless of whether the starting microstructure was annealed by CHT or annealed and recrystallised (RHT). Although the difference in strength cannot be ascribed to a detectable difference in the microstructure of the aged samples, it is thought that ageing of Ti-6Al-4V would lead to the precipitation of intermetallic nanometre-sized α_2 (Ti_3Al) particles [48,54], which could enable a form of precipitation hardening in Ti-6Al-4V.

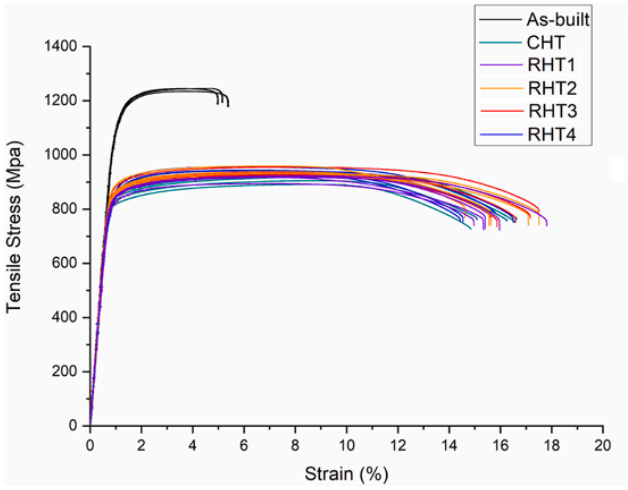

Fig. 10. Stress-strain curves of all the specimens investigated in this study.

Table 6
Comparison between microstructural features obtained after conventional and rapid heat treatment of L-PBF Ti-6Al-4V.

	Conventional heat treatment	RHTs
Microstructural constituents	α+ β	α+ β
Morphology, location and size of α and β phase	• Basketweave α+ β lamellae • α lamellae thickness: ~1.4 μm	• Continuous prior-β grain boundary α • Parallel α+ β lamellae • α lamellae thickness: ~0.6 μm
Prior-β grain morphology	• Columnar • Average width ~85 μm	• Quasi-equiaxed • Refined average width: 30–40 μm

5. Conclusion

The results presented in this work provide new insights on innovative heat treatments aimed at optimising the mechanical properties of L-PBF of Ti-6Al-4V. Rapid heating rates into the β phase field, enable the formation of refined quasi-equiaxed prior-β grains, which might be beneficial to a number of properties (including strength, ductility, fracture toughness and fatigue). This is demonstrated by the fact that although the strengthening factor associated to the basketweave microstructure is lost, rapidly heat treated (RHT'd) samples still possess a higher combination of strength and ductility than the samples that were heat treated following ASTM standards (CHT). Nevertheless, further considerations should be given to the size and morphological arrangement of the α laths, which are known to contribute significantly on the yield and deformation mode of Ti-6Al-4V. The results of this study suggest that slow equilibrium cooling from temperatures above the β transus causes the undesirable formation of α colonies and grain boundary α laths, therefore faster cooling rates (such as forced convective cooling from inert gas or quenching) should be considered in the future to develop (prior-β) refined basketweave stronger microstructures. By interpreting tensile data with a detailed microstructural investigation, the following conclusions can be drawn:

- Specimens in the as-built condition present a typical microstructure consisting of fine acicular α′ martensite in columnar prior-β grains. Samples present exceptional strength but limited ductility;
- Specimens for which a conventional heat treatment was chosen, present a basketweave equilibrium α+β microstructure encased in columnar prior-β grains (of the same size of the as-built specimens). The treatment leads to balanced tensile properties, with the recovery of ductility at the expenses of strength.
- All the proposed RHTs are effective to refine the prior-β grains. It was observed that the refinement is at its peak when the soak time is kept briefly above the β transus temperature. This is attributed to remnants of the α phase at high temperatures (up to the β transus temperature), which are thought to effectively pin and hinder extensive growth of the β phase.
- The investigated RHTs produce relatively thin α laths arranged with a colony morphology. Grain boundary α were also observed in all the specimens subject to RHTs. The α colony morphology and grain boundary α are thought to impact negatively on the tensile properties of the material investigated. Nevertheless, samples benefit from a refined prior-β grain structure, and display an increase in tensile strength whilst maintaining comparable ductility to conventionally treated Ti-6Al-4V.
- Ageing is beneficial to both RTHed and CHTed specimens suggesting that the plausible associated α_2 (Ti_3Al) precipitation hardening mechanism is not affected by the initial content in dislocations in the material or the arrangement and size of the α and β constituents.

Data availability

The data that support the findings of this study are available from the corresponding author, Marco Simonelli, upon reasonable request.

CRediT authorship contribution statement

Zhiyi Zou: Conceptualization, Methodology, Investigation, Formal analysis, Writing – original draft. **Marco Simonelli:** Conceptualization, Formal analysis, Writing – review & editing, Supervision. **Juliano Katrib:** Writing – review & editing, Supervision. **Georgios Dimitrakis:** Writing – review & editing, Supervision. **Richard Hague:** Writing – review & editing, Supervision.

Declaration of competing interest

The authors declare that they have no known competing financial interests or personal relationships that could have appeared to influence the work reported in this paper.

Acknowledgements

The work presented here has been made possible by funding provided through the University of Nottingham PhD scholarship. Special thanks to Dr Nigel Neate and Mr Martin Roe (nano- and micro-scale Research Centre, University of Nottingham) for their support with the EBSD experiments. Thanks to Dr Ryan Maclachlan (Loughborough University) for his help with the EBSD investigations and the useful discussions.

References

[1] G. Lütjering, J.C. Williams, Titanium, Springer Science & Business Media, 2007.
[2] F.H.e. Froes, Titanium : Physical Metallurgy Processing and Applications/, in: F.H. Froes (Ed.), ASM International, Materials Park, Ohio, 2015.
[3] I. Polmear, D. StJohn, J.-F. Nie, M. Qian, Light Alloys: Metallurgy of the Light Metals, Butterworth-Heinemann, Oxford, 2017.
[4] S. Liu, Y.C. Shin, Additive manufacturing of Ti6Al4V alloy: a review, Mater. Des. 164 (2019) 107552.
[5] Z. Zou, M. Simonelli, J. Katrib, G. Dimitrakis, R. Hague, Refinement of the grain structure of additive manufactured titanium alloys via epitaxial recrystallization enabled by rapid heat treatment, Scripta Mater. 180 (2020) 66–70.
[6] B.E. Carroll, T.A. Palmer, A.M. Beese, Anisotropic tensile behavior of Ti–6Al–4V components fabricated with directed energy deposition additive manufacturing, Acta Mater. 87 (2015) 309–320.
[7] H. Ali, L. Ma, H. Ghadbeigi, K. Mumtaz, In-situ residual stress reduction, martensitic decomposition and mechanical properties enhancement through high temperature powder bed pre-heating of Selective Laser Melted Ti6Al4V, Mater. Sci. Eng., A 695 (2017) 211–220.
[8] L. Thijs, F. Verhaeghe, T. Craeghs, J.V. Humbeeck, J.-P. Kruth, A study of the microstructural evolution during selective laser melting of Ti–6Al–4V, Acta Mater. 58 (9) (2010) 3303–3312.
[9] M. Shunmugavel, A. Polishetty, R. Singh, G. Littlefair, A comparative study of mechanical properties and machinability of wrought and additive manufactured (selective laser melting) titanium alloy – Ti-6Al-4V, Rapid Prototyp. J. 23 (6) (2017) 1051–1056.
[10] M. Simonelli, Y.Y. Tse, C. Tuck, Effect of the build orientation on the mechanical properties and fracture modes of SLM Ti–6Al–4V, Mater. Sci. Eng., A 616 (2014) 1–11.
[11] W. Xu, M. Brandt, S. Sun, J. Elambasseril, Q. Liu, K. Latham, K. Xia, M. Qian, Additive manufacturing of strong and ductile Ti–6Al–4V by selective laser melting via in situ martensite decomposition, Acta Mater. 85 (2015) 74–84.
[12] H. Shipley, D. McDonnell, M. Culleton, R. Coull, R. Lupoi, G. O'Donnell, D. Trimble, Optimisation of process parameters to address fundamental challenges during selective laser melting of Ti-6Al-4V: a review, Int. J. Mach. Tool Manufact. 128 (2018) 1–20.
[13] W. Xu, S. Sun, J. Elambasseril, Q. Liu, M. Brandt, M. Qian, Ti-6Al-4V additively manufactured by selective laser melting with superior mechanical properties, JOM 67 (3) (2015) 668–673.
[14] A.H. Baker, P.C. Collins, J.C. Williams, New nomenclatures for heat treatments of additively manufactured titanium alloys, JOM 69 (7) (2017) 1221–1227.

[15] X.-Y. Zhang, G. Fang, S. Leeflang, A.J. Böttger, A. Zadpoor, J. Zhou, Effect of subtransus heat treatment on the microstructure and mechanical properties of additively manufactured Ti-6Al-4V alloy, J. Alloys Compd. 735 (2018) 1562–1575.
[16] T. Vilaro, C. Colin, J.D. Bartout, As-Fabricated and heat-treated microstructures of the Ti-6Al-4V alloy processed by selective laser melting, Metall. Mater. Trans. 42 (10) (2011) 3190–3199.
[17] A.M. Beese, B.E. Carroll, Review of mechanical properties of Ti-6Al-4V made by laser-based additive manufacturing using powder feedstock, JOM 68 (3) (2016) 724–734.
[18] ASTM, Standard Specification for Additive Manufacturing Titanium-6 Aluminum-4 Vanadium with Powder Bed Fusion, ASTM International, 2014.
[19] ASTM, Standard Specification for Additive Manufacturing Titanium-6 Aluminum-4 Vanadium ELI (Extra Low Interstitial); with Powder Bed Fusion, ASTM International, 2014.
[20] B. Vrancken, L. Thijs, J.-P. Kruth, J. Van Humbeeck, Heat treatment of Ti6Al4V produced by selective laser melting: microstructure and mechanical properties, J. Alloys Compd. 541 (2012) 177–185.
[21] L.Y. Chen, J.C. Huang, C.H. Lin, C.T. Pan, S.Y. Chen, T.L. Yang, D.Y. Lin, H. K. Lin, J.S.C. Jang, Anisotropic response of Ti-6Al-4V alloy fabricated by 3D printing selective laser melting, Mater. Sci. Eng., A 682 (2017) 389–395.
[22] M.-W. Wu, P.-H. Lai, J.-K. Chen, Anisotropy in the impact toughness of selective laser melted Ti–6Al–4V alloy, Mater. Sci. Eng., A 650 (2016) 295–299.
[23] Z. Zhao, J. Chen, H. Tan, G. Zhang, X. Lin, W. Huang, Achieving superior ductility for laser solid formed extra low interstitial Ti-6Al-4V titanium alloy through equiaxial alpha microstructure, Scripta Mater. 146 (2018) 187–191.
[24] R. Sabban, S. Bahl, K. Chatterjee, S. Suwas, Globularization using heat treatment in additively manufactured Ti-6Al-4V for high strength and toughness, Acta Mater. 162 (2019) 239–254.
[25] K. AmirMahyar, G. Ian, G. Moshe, L. Guy, On the role of different annealing heat treatments on mechanical properties and microstructure of selective laser melted and conventional wrought Ti-6Al-4V, Rapid Prototyp. J. 23 (2) (2017) 295–304.
[26] G.F. Vander Voort, A. Roósz, Measurement of the interlamellar spacing of pearlite, Metallography 17 (1) (1984) 1–17.
[27] H. Abrams, Grain size measurement by the intercept method, Metallography 4 (1) (1971) 59–78.
[28] M. Simonelli, Y.Y. Tse, C. Tuck, On the texture formation of selective laser melted Ti-6Al-4V, Metall. Mater. Trans. 45 (6) (2014) 2863–2872.
[29] I. ASTM, ASTM E8/E8M-16a: Standard Test Methods for Tension Testing of Metallic Materials, ASTM International, West Conshohocken, PA, USA, 2016.
[30] F. Luca, M. Emanuele, R. Pierfrancesco, M. Alberto, H. Simon, W. Konrad, Ductility of a Ti-6Al-4V alloy produced by selective laser melting of prealloyed powder, Rapid Prototyp. J. 16 (6) (2010) 450–459.
[31] S.L.R. da Silva, L.O. Kerber, L. Amaral, C.A. dos Santos, X-ray diffraction measurements of plasma-nitrided Ti–6Al–4V, Surf. Coating. Technol. 116–119 (1999) 342–346.
[32] S.Q. Wu, Y.J. Lu, Y.L. Gan, T.T. Huang, C.Q. Zhao, J.J. Lin, S. Guo, J.X. Lin, Microstructural evolution and microhardness of a selective-laser-melted Ti–6Al–4V alloy after post heat treatments, J. Alloys Compd. 672 (2016) 643–652.
[33] P. Tao, J. Zhong, H. Li, Q. Hu, S. Gong, Q. Xu, Microstructure, mechanical properties, and constitutive models for Ti–6Al–4V alloy fabricated by selective laser melting (SLM), Metals 9 (4) (2019) 447.
[34] N.V. Kazantseva, I.V. Ezhov, N.I. Vinogradova, M.V. Il'inykh, A.S. Fefelov, D.I. Davydov, O.A. Oleneva, M.S. Karabanalov, Effect of built geometry on the microstructure and strength characteristics of the Ti–6Al–4V alloy prepared by the selective laser melting, Phys. Met. Metallogr. 119 (11) (2018) 1079–1086.
[35] M. Neikter, P. Åkerfeldt, R. Pederson, M.L. Antti, V. Sandell, Microstructural characterization and comparison of Ti-6Al-4V manufactured with different additive manufacturing processes, Mater. Char. 143 (2018) 68–75.
[36] J.J.S. Dilip, S. Zhang, C. Teng, K. Zeng, C. Robinson, D. Pal, B. Stucker, Influence of processing parameters on the evolution of melt pool, porosity, and microstructures in Ti-6Al-4V alloy parts fabricated by selective laser melting, Progr. Addit. Manufac. 2 (3) (2017) 157–167.
[37] A.E. Wilson-Heid, Z. Wang, B. McCornac, A.M. Beese, Quantitative relationship between anisotropic strain to failure and grain morphology in additively manufactured Ti-6Al-4V, Mater. Sci. Eng., A 706 (2017) 287–294.
[38] G.A. Sargent, K.T. Kinsel, A.L. Pilchak, A.A. Salem, S.L. Semiatin, Variant selection during cooling after beta annealing of Ti-6Al-4V ingot, Mater. Metall. Mater. Trans. A 43 (10) (2012) 3570–3585.
[39] R. Shi, Y. Wang, Variant selection during α precipitation in Ti–6Al–4V under the influence of local stress – a simulation study, Acta Mater. 61 (16) (2013) 6006–6024.
[40] D. Zhang, L. Wang, H. Zhang, A. Maldar, G. Zhu, W. Chen, J.-S. Park, J. Wang, X. Zeng, Effect of heat treatment on the tensile behavior of selective laser melted Ti-6Al-4V by in situ X-ray characterization, Acta Mater. 189 (2020) 93–104.
[41] P. Kumar, U. Ramamurty, Microstructural optimization through heat treatment for enhancing the fracture toughness and fatigue crack growth resistance of selective laser melted Ti6Al4V alloy, Acta Mater. 169 (2019) 45–59.
[42] P. Guo, Y. Zhao, W. Zeng, Q. Hong, The effect of microstructure on the mechanical properties of TC4-DT titanium alloys, Mater. Sci. Eng., A 563 (2013) 106–111.
[43] A. Zafari, K. Xia, High Ductility in a fully martensitic microstructure: a paradox in a Ti alloy produced by selective laser melting, Mater. Res. Lett. 6 (11) (2018) 627–633.
[44] S. Cao, Q. Hu, A. Huang, Z. Chen, M. Sun, J. Zhang, C. Fu, Q. Jia, C.V.S. Lim, R.R. Boyer, Y. Yang, X. Wu, Static coarsening behaviour of lamellar microstructure in selective laser melted Ti–6Al–4V, J. Mater. Sci. Technol. 35 (8) (2019) 1578–1586.
[45] B.J. Hayes, B.W. Martin, B. Welk, S.J. Kuhr, T.K. Ales, D.A. Brice, I. Ghamarian, A.H. Baker, C.V. Haden, D.G. Harlow, H.L. Fraser, P.C. Collins, Predicting tensile properties of Ti-6Al-4V produced via directed energy deposition, Acta Mater. 133 (2017) 120–133.
[46] I. Ghamarian, B. Hayes, P. Samimi, B.A. Welk, H.L. Fraser, P.C. Collins, Developing a phenomenological equation to predict yield strength from composition and microstructure in β processed Ti-6Al-4V, Mater. Sci. Eng., A 660 (2016) 172–180.
[47] E. Lee, Microstructure Evolution and Microstructure/mechanical Properties Relationships in α+ β Titanium Alloys, 2004.
[48] H. Galarraga, R.J. Warren, D.A. Lados, R.R. Dehoff, M.M. Kirka, P. Nandwana, Effects of heat treatments on microstructure and properties of Ti-6Al-4V ELI alloy fabricated by electron beam melting (EBM), Mater. Sci. Eng., A 685 (2017) 417–428.
[49] J. Haubrich, J. Gussone, P. Barriobero-Vila, P. Kürnsteiner, E.A. Jägle, D. Raabe, N. Schell, G. Requena, The role of lattice defects, element partitioning and intrinsic heat effects on the microstructure in selective laser melted Ti-6Al-4V, Acta Mater. 167 (2019) 136–148.
[50] O.M. Ivasishin, R.V. Teliovich, Potential of rapid heat treatment of titanium alloys and steels, Mater. Sci. Eng., A 263 (2) (1999) 142–154.
[51] Y. Chong, T. Bhattacharjee, J. Yi, A. Shibata, N. Tsuji, Mechanical properties of fully martensite microstructure in Ti-6Al-4V alloy transformed from refined beta grains obtained by rapid heat treatment (RHT), Scripta Mater. 138 (2017) 66–70.
[52] A. Moridi, A.G. Demir, L. Caprio, A.J. Hart, B. Previtali, B.M. Colosimo, Deformation and failure mechanisms of Ti–6Al–4V as built by selective laser melting, Mater. Sci. Eng., A 768 (2019) 138456.
[53] K.N. Kumar, P. Muneshwar, S.K. Singh, A.K. Jha, B. Pant, K.M. George, Effect of grain boundary alpha on mechanical properties of Ti5.4Al3Mo1V alloy, JOM 67 (6) (2015) 1265–1272.
[54] D.-G. Lee, S. Lee, C.S. Lee, Quasi-static and dynamic deformation behavior of Ti–6Al–4V alloy containing fine α2-Ti3Al precipitates, Mater. Sci. Eng., A 366 (1) (2004) 25–37.